

Data report: clay mineralogical composition of northern Cascadia margin sediments, IODP Expedition 311¹

Danièle Bartier,² Marie-Madeleine Blanc-Valleron,² Jean Marie Rouchy,² and Catherine Pierre³

Chapter contents

Abstract	1
Introduction	1
X-ray diffraction methods	2
Results	2
Conclusion	3
Acknowledgments	4
References	4
Figures	5
Table	12

Abstract

The clay mineralogical semiquantitative composition of 186 samples of hemipelagic sediments, turbiditic sediments, and authigenic carbonates from Integrated Ocean Drilling Program Sites U1325–U1329, northern Cascadia margin, were determined by X-ray diffraction analyses. Oriented aggregates of clay-sized fractions were analyzed to estimate the relative percentages of smectite, illite, chlorite, kaolinite, and illite/vermiculite mixed layers. Illite/vermiculite mixed layers were observed for the first time in this area. Clay mineral assemblages show only modest long-term variations with no significant differences among Sites U1325–U1329. Variations in clay mineral assemblages are supposed to be mostly related to differences between hemipelagic sediments and turbiditic sediments. The sampling resolution and the age control are not good enough to define or recognize any climate control indicators in the clay mineral record.

Introduction

The Juan de Fuca plate is being subducted obliquely beneath the North American plate along the Washington, Oregon, and northern California continental margins. The Cascadia accretionary prism evolved in response to this oblique subduction. It is composed of folded and faulted abyssal plain turbidites and hemipelagic sediments (Kulm and Fowler, 1974; MacKay et al., 1992). In the northern section of the Cascadia margin, a gas hydrate-related bottom-simulating reflector occurs in a 30 km wide band parallel to the coast beneath much of the continental slope (Fig. F1A). Integrated Ocean Drilling Program Expedition 311 follows Ocean Drilling Program Legs 146 (north Hydrate Ridge) and 204 (south Hydrate Ridge) drilling campaigns in the Cascadia margin area to characterize gas hydrate processes. To constrain the distribution and concentration of gas hydrate in this region, four sites (U1326, U1325, U1327, and U1329) were drilled along a southwest-northeast transect during Expedition 311, from an uplifted ridge near the base of the continental slope (Site U1326) to near the edge of the continental shelf (Site U1329); a fifth site (U1328), representing a cold seep site with active fluid and gas flow, was also drilled (Fig. F1B) (see the “Expedition 311 Summary” chapter). This data report describes the clay assemblages identified by X-ray diffraction of 186 turbiditic sediments, hemipelagic sedi-

¹Bartier, D., Blanc-Valleron, M.-M., Rouchy, J.M., and Pierre, C., 2008. Data report: clay mineralogical composition of northern Cascadia margin sediments, IODP Expedition 311. In Riedel, M., Collett, T.S., Malone, M.J., and the Expedition 311 Scientists, *Proc. IODP*, 311: Washington, DC (Integrated Ocean Drilling Program Management International, Inc.).

doi:10.2204/iodp.proc.311.208.2008

²UMR 5143 CNRS, Département Histoire de la Terre—Géologie, Muséum National d’Histoire Naturelle, 43 rue Buffon, 75005 Paris, France.

Correspondence author: bartier@mnhn.fr

³CNRS-LOCEAN, Université Pierre et Marie Curie, 4 Place Jussieu, 75252 Paris Cedex 05, France.



ments, and authigenic carbonates. The aim was originally to investigate potential modifications of clay mineral assemblages through sites, lithology, depth, and gas hydrate occurrence.

X-ray diffraction methods

Sample preparation

The sample preparation method used in this study is described in Holtzapffel (1985). Separation of clay-sized fractions (<2 µm) started with a gentle crushing of samples and decalcification using a solution of 0.2N HCl in an Erlenmeyer flask. The preparation was washed with distilled water, and clay deflocculation was obtained through repeated centrifuging (2500 revolutions per minute [rpm] for 3 min). After each centrifugation, water was eliminated and the plug was resuspended in distilled water. Generally, three to six centrifugation-suspension cycles were necessary until deflocculation. After transferring the suspended sediment to a glass beaker and vigorously shaking it, the clay fraction was separated by decantation using settling time based on Stoke's law. The extracted clay fraction was then centrifuged at 3500 rpm for 40 min, and, finally, the clay plug was used to make an oriented clay glass slide. X-ray diffraction analyses were conducted on air-dried clay slides after saturation with ethylene glycol (at least 24 h) and after heating at 490°C for 2 h.

X-ray diffraction parameters

X-ray diffractograms were obtained at the Muséum National d'Histoire Naturelle of Paris using a Siemens D500 X-ray diffractometer with CuK α radiation (1.54 Å) and Ni filter. Instrument parameters were set to 40 kV accelerating voltage and 30 mA current. Scans were run from 2° to 40°2θ with a scanning step size of 0.02°2θ and counting time of 4 s. X-ray diagrams were studied using MacDiff (version 4.2.5) software (servermac.geologie.uni-frankfurt.de/Staff/Homepages/Petschick/RainerE.html) in order to establish the background line, smooth counts, correct peak positions (using quartz [100] peak at 4.24 Å), and compute integrated peak areas (total counts). The semiquantitative clay mineral proportions were estimated from the glycolated pattern. Clay mineral identification was made according to the position of the 001 series of basal reflections (Brown and Brindley, 1980). X-ray diffraction analyses allowed us to identify smectite, illite, chlorite, kaolinite, and some random mixed-layered illite/vermiculite (I/V). These I/V mixed layers are

characterized in air-dried conditions by a broad peak ranging from 10 to 13 Å, with a maximum intensity at ~12 Å. This peak is not altered in position or intensity by glycol saturation but collapses to 10 Å after heating (Fig. F2). In order to allow comparisons with published data from the northern Pacific region (Duncan et al., 1970; Karlin, 1980; Underwood, 2002; Underwood and Torres, 2006), the integrated areas were multiplied by weighting factors (Biscaye, 1965) and normalized to 100%. Weighting factors are 4 for illite, 2 for kaolinite + chlorite, and 1 for smectite (Biscay, 1965); we chose to use 1 for I/V in order to compare results with those already published for this area (in which no I/V was detected), so percentages are only slightly "mathematically" modified. Chlorite and kaolinite were differentiated using the 3.54 Å/3.57 Å peak ratio. The smectite term corresponds to a random R0 smectite/illite mixed layer (R0 I/S) and the amount of expandable layers was calculated based on the valley/peak height (v/p) ratio (after Biscay, 1965), the difference in the height of the base line from the high and low 2θ sides of the 5.2°2θ peak. Abacus allows consideration of the percentage of smectite portion from the measure of the v/p parameter (the saddle-peak method; Rettke, 1981). The estimated analytical precision is ±5%.

Results

A total of 186 samples of hemipelagic samples, turbiditic samples, and carbonate concretion samples were analyzed in this study. Figures F3, F4, F5, F6, and F7 display downhole variations of clay minerals for each site. The X-ray diffraction data are illustrated in Table T1.

As previously stated, we used the factors of Biscay (1965) to estimate semiquantitative clay mineral percentages in order to compare our results with already published data. However, we must note that using these factors and 1 as the factor for I/V "minimizes" the proportion of I/V compared to semiquantitative estimates based on other methods described in Holtzapffel (1985). I/V mixed layers were never observed offshore Oregon (e.g., Karlin, 1980; Underwood, 2002; Gràcia et al., 2006; Underwood and Torres, 2006), whereas they are present in Pleistocene northwestern Atlantic sediments and relate to interglacial periods (e.g., Vanderaverde et al., 2000). Vermiculite and random mixed-layer minerals were also described in late Pleistocene sediments of Vancouver Island (Blaise, 1989). The expandability values in R0 I/S for each site are quite similar (mean = ~60%–65%; lower values are obviously observed in smec-



ite-poor samples). Therefore, as with Underwood and Torres (2006), we suppose that the expandable clay is probably detrital in origin with small amounts of interlayered illite.

Site U1326

Site U1326 is located on top of the first uplifted ridge of accreted sediments at the far western downslope end of the transect. Thirty-three samples from lithostratigraphic Unit I (Hole U1326C), Unit II (Holes U1326C and U1326D), and Unit III (Hole U1326D) were analyzed (Table T1; Fig. F3). Three samples analyzed for Unit I show a similar clay assemblage composed of smectite (19%), illite (42%), chlorite (28%), and kaolinite (12%). There is an anticorrelation between smectite and illite in Unit II and between illite and chlorite (+ kaolinite) in Unit III. Moreover, as noted by [Bahr et al.](#), there is a trend toward higher illite and chlorite (+ kaolinite) contents in the lower part of Unit II and all of Unit III. The lower smectite content in Unit III is accompanied by a slight decrease in the amount of expandable layers (Percent expand in Table T1). The authigenic carbonate-rich sample at 235.90 meters below seafloor (mbsf) does not show any particular clay content.

Site U1325

Site U1325 is located within the first slope basin in the southwestern part of the transect. Thirty-five samples from lithostratigraphic Units IA, IB, II, and III (Hole U1325B) and Unit IV (Hole U1325C) were analyzed. As for Site U1326, clay mineral assemblages are composed of smectite, illite, chlorite, kaolinite, and I/V (Table T1; Fig. F4). No global trend was noted except in Units I-II, in which the observed moderate anticorrelation between smectite and illite could be linked to sediment grain size, turbiditic samples being more illitic, whereas hemipelagic samples are more smectitic. Unit IV (as Unit III for Site U1326) appears slightly richer in chlorite and I/V than Units I-III and poorer in smectite. The authigenic carbonate-rich sample analyzed in Unit III does not show any particular clay content.

Site U1327

Site U1327 is located on the midcontinental slope off Vancouver Island, several hundred meters from Site 889 (Leg 146). Forty-two samples from lithostratigraphic Unit I (Hole U1327C), Unit II (Holes U1327C and U1327D), and Unit III (Hole U1327C) were analyzed (Table T1; Fig. F5). Units I-III display an anticorrelation between smectite and illite related

to sediment grain size. Unit III is slightly richer in illite and poorer in smectite than Units I and II, whereas Unit I displays a little more I/V. Six authigenic carbonate-rich samples were analyzed (one in Unit I, four in Unit II, and one in Unit III) with no particular clay content.

Site U1328

Site U1328 is located 3.7 km southeast of Site U1327 on the midcontinental slope off Vancouver Island. Forty-four samples from lithostratigraphic Unit I (Holes U1328B and U1328C), Unit II (Hole U1328C), and Unit III (Hole U1328C) were analyzed (Table T1; Fig. F6). As for the precedent sites, an anticorrelation trend between smectite and illite, related to sediment grain size, was observed. The most smectitic samples (and poorest in illite) are observed at the base of Unit I between 105 and 130 mbsf. Lithostratigraphic Unit II is slightly richer in illite and poorer in smectite than Units I and III. Four authigenic carbonate-rich samples were analyzed in Unit III with no particular clay content.

Site U1329

Site U1329 is the easternmost and shallowest site of the transect. Moreover, it is the only site to display Miocene sediments occurring in discordance below Pleistocene sediments. Twenty-seven samples from lithostratigraphic Units I-III (Hole U1328C) were analyzed (Table T1; Fig. F7). From 0.74 to 35.35 mbsf the clay content of samples is characterized by the lack of kaolinite (all of Unit I and the first sample of Unit II). Lithostratigraphic Unit I appears also slightly poorer in smectite than Units II and III. Globally, an anticorrelation trend between smectite and illite fractions is also observed in the three units. Compared to Pleistocene sediments, Miocene sediments are slightly richer in smectite and kaolinite and poorer in illite and chlorite.

Conclusion

At Sites U1325-U1329 of Expedition 311, the clay mineral assemblages are composed of smectite, illite, chlorite, kaolinite, and illite-vermiculite (I/V) mixed-layers. I/V layers have not been observed in the Cascadia margin area (e.g., Karlin, 1980; Underwood and Torres, 2006), whereas they are present in Pleistocene northwestern Atlantic sediments (e.g., Vandevoort et al., 2000) and are related to interglacial periods. However, in this study, the sampling resolution and the age control are not good enough to de-



fine or recognize any climate control in the clay mineral record.

Clay mineral variations are slight and probably partly due to the natural heterogeneity of the clay-sized sediment budget. Nevertheless, it is possible to see some differences between sites and between units in the same site. Lithostratigraphic Unit I at Site U1329 does not contain kaolinite. The lowest smectite contents are observed in lithostratigraphic Unit IV at Site U1325 and Unit III at Site U1326, whereas higher values are recorded in the Miocene of lithostratigraphic Unit III at Site U1329. In all sites, a global anticorrelation trend between illite and smectite fractions is observed. This trend could be correlated to sediment grain size, hemipelagic sediments being slightly richer in smectite and turbiditic samples slightly enriched in illite. In the samples studied, there is no evidence of diagenetic impact of gas hydrate and/or carbonate diagenesis occurrence on the clay mineral fraction.

Acknowledgments

The authors would like to thank Pierre Clément and Anne-Marie Brunet (MNHN, Paris, France) for help with sample processing and XRD analyses and Liviu Giosans and editor Lorri Peters for their careful review of the manuscript. This research used samples and/or data provided by the Integrated Ocean Drilling Program (IODP). Funding for this research was provided by an Eclipse II grant of the CNRS.

References

- Biscaye, P.E., 1965. Mineralogy and sedimentation of recent deep-sea clay in the Atlantic Ocean and adjacent seas and oceans. *Geol. Soc. Am. Bull.*, 76(7):803–831. [doi:10.1130/0016-7606\(1965\)76\[803:MASORD\]2.0.CO;2](https://doi.org/10.1130/0016-7606(1965)76[803:MASORD]2.0.CO;2)
- Blaise, B., 1989. Clay-mineral assemblages from Late Quaternary deposits on Vancouver Island, southwestern British Columbia, Canada. *Quat. Res.*, 31(1):41–56. [doi:10.1016/0033-5894\(89\)90084-7](https://doi.org/10.1016/0033-5894(89)90084-7)
- Brown, G., and Brindley, G.W., 1980. X-ray diffraction procedures for clay mineral identification. In Brindley, G.W., and Brown, G. (Eds.), *Crystal Structures of Clay Minerals and Their X-ray Identification*. Mineral. Soc. Monogr. London, 5:305–359.
- Duncan, J.R., Kulm, L.D., and Griggs, G.B., 1970. Clay mineral composition of late Pleistocene and Holocene sediments of Cascadia Basin, northeastern Pacific Ocean. *J. Geol.*, 78:213–221.
- Gràcia, E., Martínez-Ruiz, F., Piñero, E., Larrasoña, J.C., Vizcaino, A., and Ercilla, G., 2006. Data report: grain-size and bulk and clay mineralogy of sediments from the summit and flanks of southern Hydrate Ridge, Sites 1244–1250, ODP Leg 204. In Tréhu, A.M., Bohrmann, G., Torres, M.E., and Colwell, F.S. (Eds.), *Proc. ODP, Sci. Results*, 204: College Station, TX (Ocean Drilling Program), 1–19. [doi:10.2973/odp.proc.sr.204.110.2006](https://doi.org/10.2973/odp.proc.sr.204.110.2006)
- Holtzapffel, T., 1985. Les minéraux argileux: préparation, analyse diffractométrique et détermination. *Publ. Soc. Geol. Nord.*, 12.
- Karlin, R., 1980. Sediment sources and clay mineral distributions off the Oregon coast. *J. Sediment. Petrol.*, 50:543–560.
- Kulm, L.D., and Fowler, G.A., 1974. Oregon continental margin structure and stratigraphy: a test of the imbricate thrust model. In Burke, C.A., and Drake, C.L. (Eds.), *The Geology of Continental Margins*: New York (Springer), 261–284.
- MacKay, M.E., Moore, G.F., Cochrane, G.R., Moore, J.C., and Kulm, L.D., 1992. Landward vergence and oblique structural trends in the Oregon margin accretionary prism: implications and effect on fluid flow. *Earth Planet. Sci. Lett.*, 109(3–4):477–491. [doi:10.1016/0012-821X\(92\)90108-8](https://doi.org/10.1016/0012-821X(92)90108-8)
- Rettke, R.C., 1981. Probable burial diagenetic and provenance effects on Dakota Group clay mineralogy, Denver Basin. *J. Sediment. Petrol.*, 51:541–551.
- Underwood, M., and Torres, M., 2006. Data report: composition of clay minerals from hemipelagic sediments at Hydrate Ridge, Cascadia subduction zone. In Tréhu, A.M., Bohrmann, G., Torres, M.E., and Colwell, F.S. (Eds.), *Proc. ODP, Sci. Results*, 204: College Station TX (Ocean Drilling Program), 1–15. [doi:10.2973/odp.proc.sr.204.127.2006](https://doi.org/10.2973/odp.proc.sr.204.127.2006)
- Underwood, M.B., 2002. Strike-parallel variations in clay minerals and fault vergence in the Cascadia subduction zone. *Geology*, 30(2):155–158. [doi:10.1130/0091-7613\(2002\)030<0155:SPVICM>2.0.CO;2](https://doi.org/10.1130/0091-7613(2002)030<0155:SPVICM>2.0.CO;2)
- Vanderaverbeet, P., Bout-Roumazeilles, V., Fagel, N., Chamley, H., and Deconinck, J.F., 2000. Significance of random illite-vermiculite mixed layers in Pleistocene sediments of the northwestern Atlantic Ocean. *Clay Miner.*, 35(4):679–691. [doi:10.1180/000985500547133](https://doi.org/10.1180/000985500547133)

Initial receipt: 26 June 2008

Acceptance: 5 September 2008

Publication: 17 November 2008

MS 311-208



Figure F1. A. Plate tectonic setting of the Cascadia margin with general location of the drilling transect near previous ODP Sites 889/890. A bottom-simulating reflector is present on ~50% of the midcontinental slope, as denoted by the shaded area (see the “[Expedition 311 summary](#)” chapter). B. Multibeam bathymetry map along the transect across the accretionary prism, showing the location of the drilling transect (Sites U1326, U1325, U1327, and U1329), cold vent Site U1328, and multichannel seismic (MCS) Line 89-08 (Courtesy of D. Kelley, J. Delaney, and D. Glickson, University of Washington; C. Barnes, C. Katnick, Neptune Canada, University of Victoria; funded by the University of Washington and the W.M. Keck Foundation).

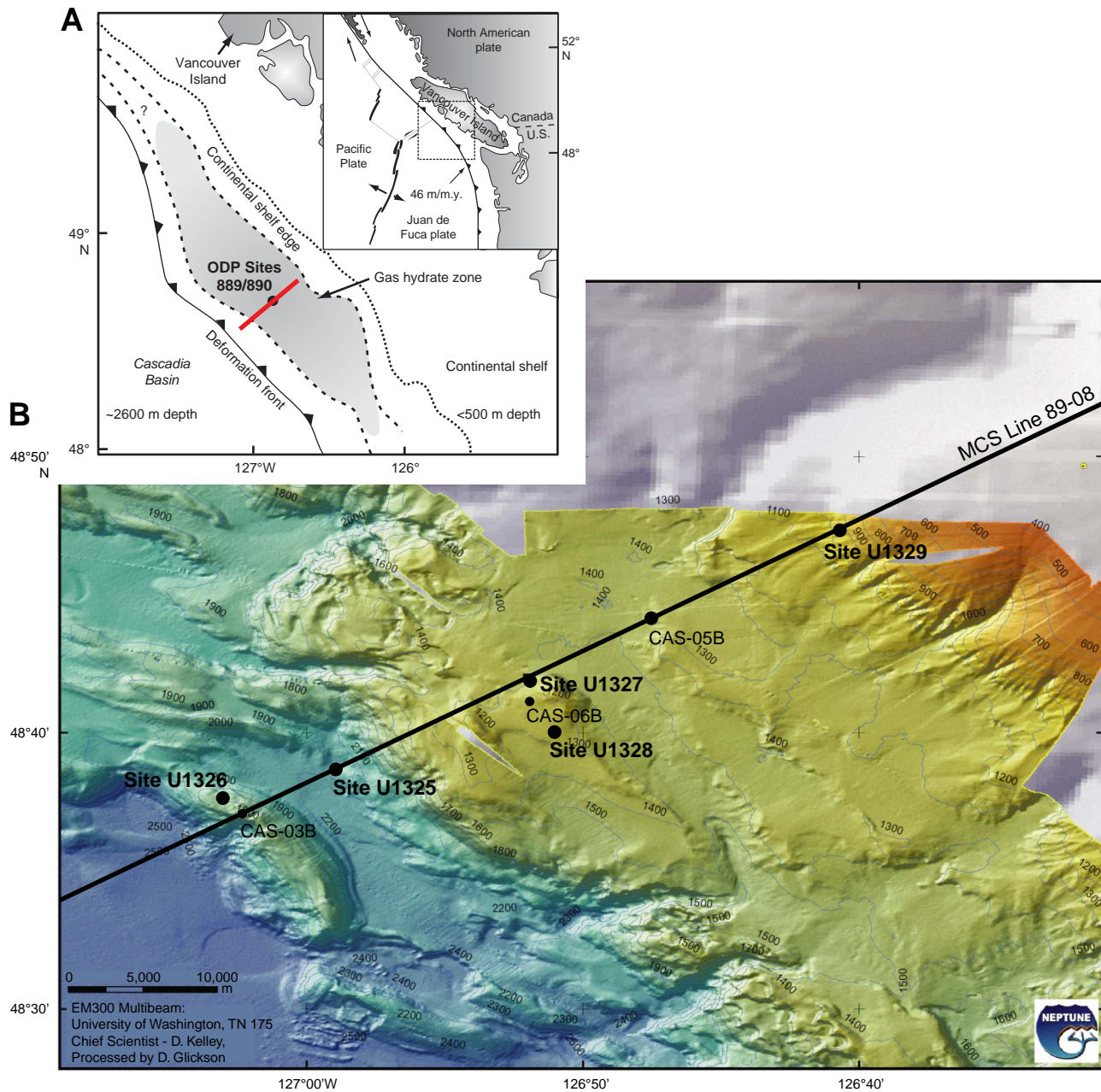


Figure F2. Selected X-ray diffractograms of Sample 311-U1326D-8X-3, 75–77 cm, showing the presence of illite/vermiculite (I/V) in the clay size fraction. Sm = smectite, Chl = chlorite, Ill = illite, Amp = amphibole, Kaol = kaolinite, Fd = feldspar, Qtz = quartz.

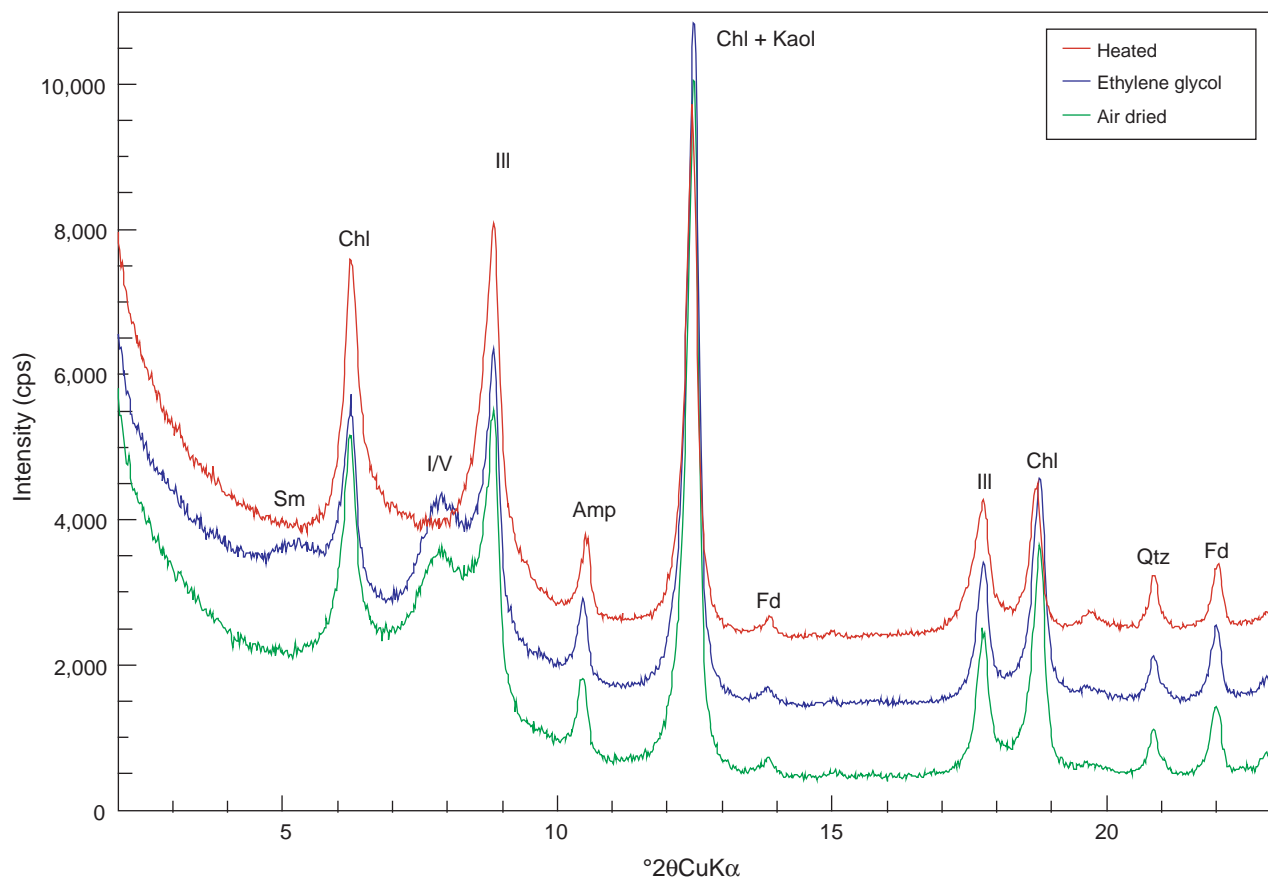


Figure F3. Downhole variations of clay minerals in sediment and authigenic carbonate samples, Site U1326. BGHSZ = bottom gas hydrate stability zone. I/V = illite/vermiculite.

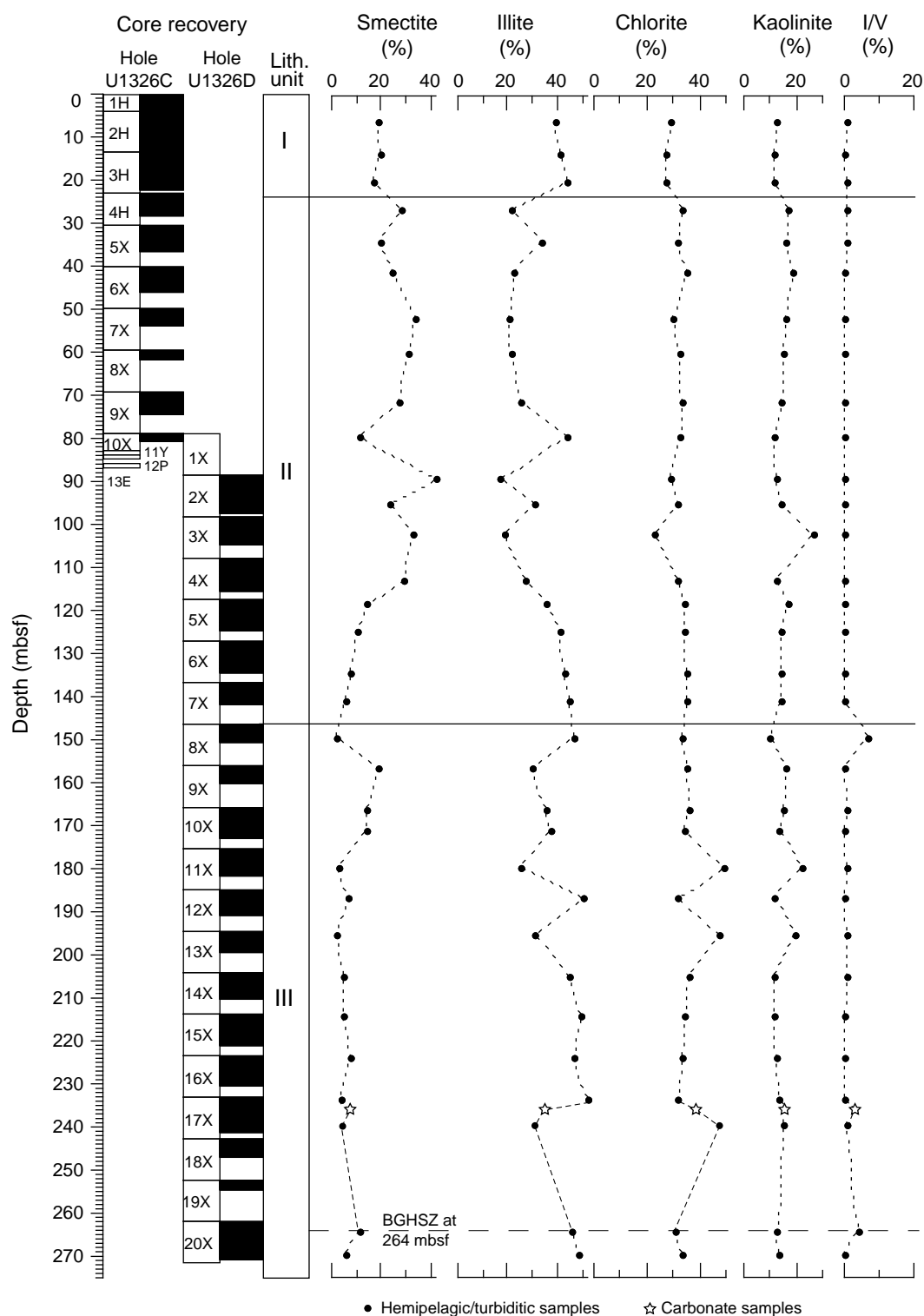


Figure F4. Downhole variations of clay minerals in sediment and authigenic carbonate samples, Site U1325. BGHSZ = bottom gas hydrate stability zone. I/V = illite/vermiculite.

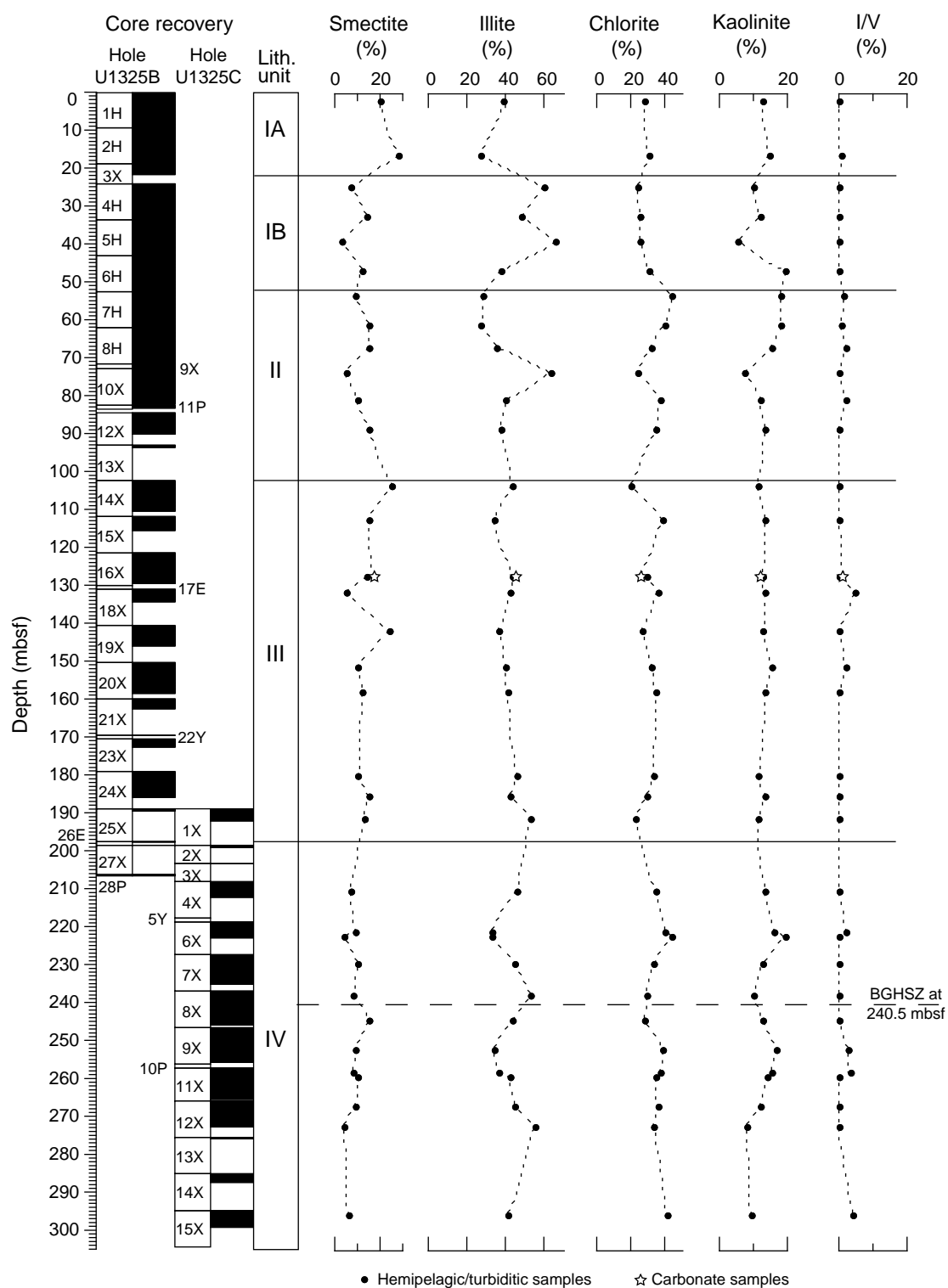


Figure F5. Downhole variations of clay minerals in sediment and authigenic carbonate samples, Site U1327. BGHSZ = bottom gas hydrate stability zone. I/V = illite/vermiculite.

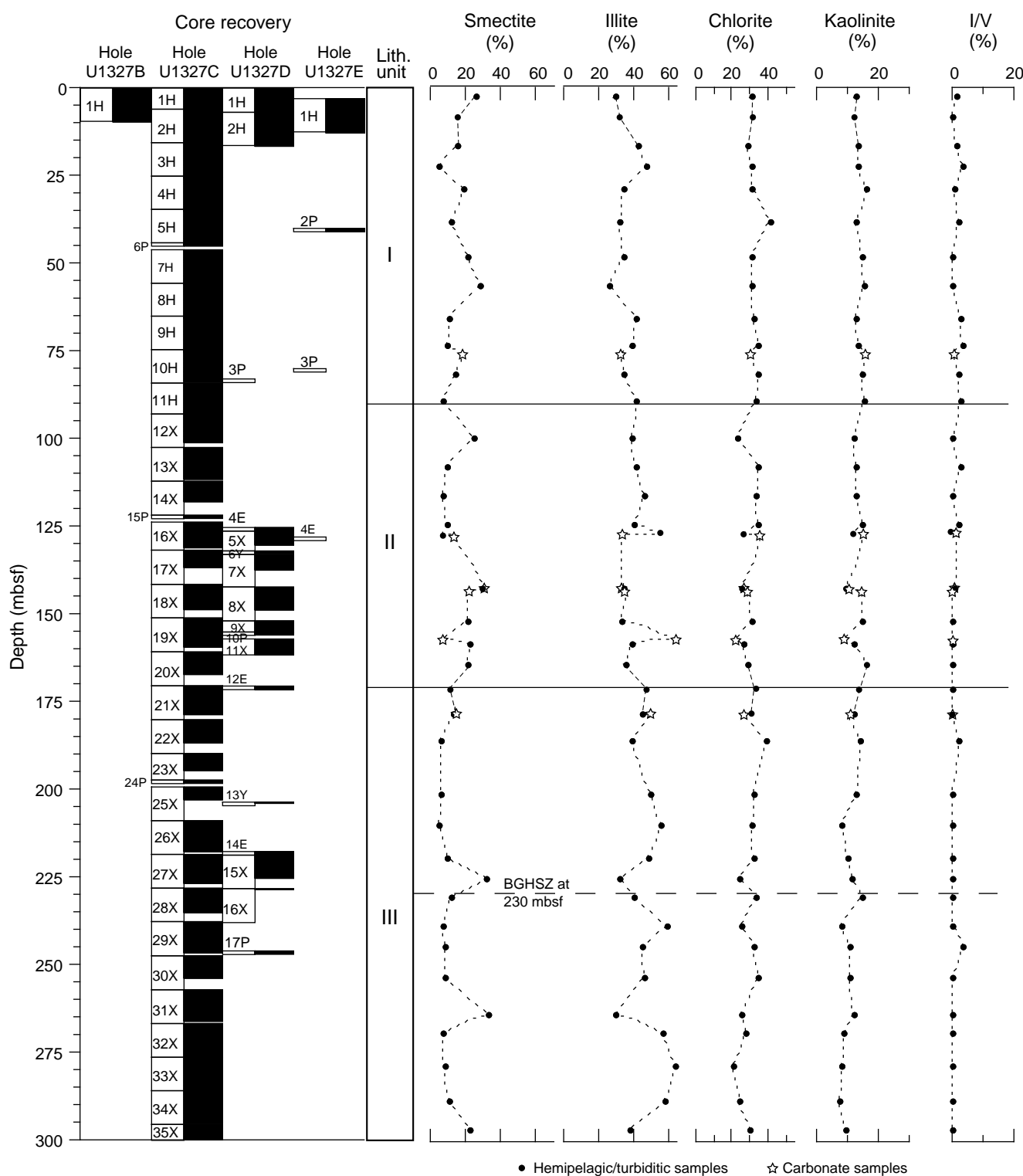


Figure F6. Downhole variations of clay minerals in sediment and authigenic carbonate samples, Site U1328. BGHSZ = bottom gas hydrate stability zone. I/V = illite/vermiculite.

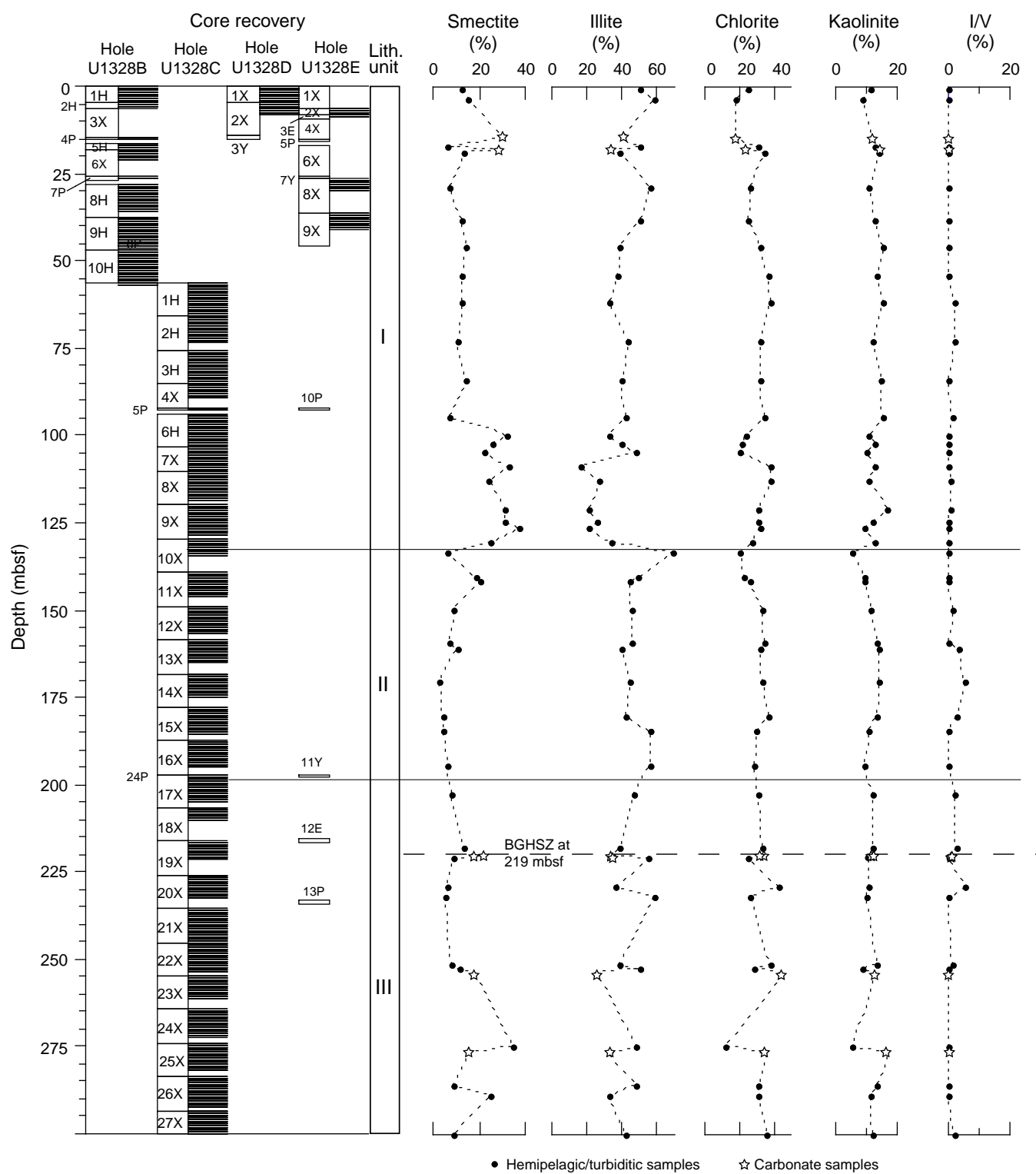


Figure F7. Downhole variations of clay minerals in sediment, Site U1329. BGHSZ = bottom gas hydrate stability zone. I/V = illite/vermiculite.

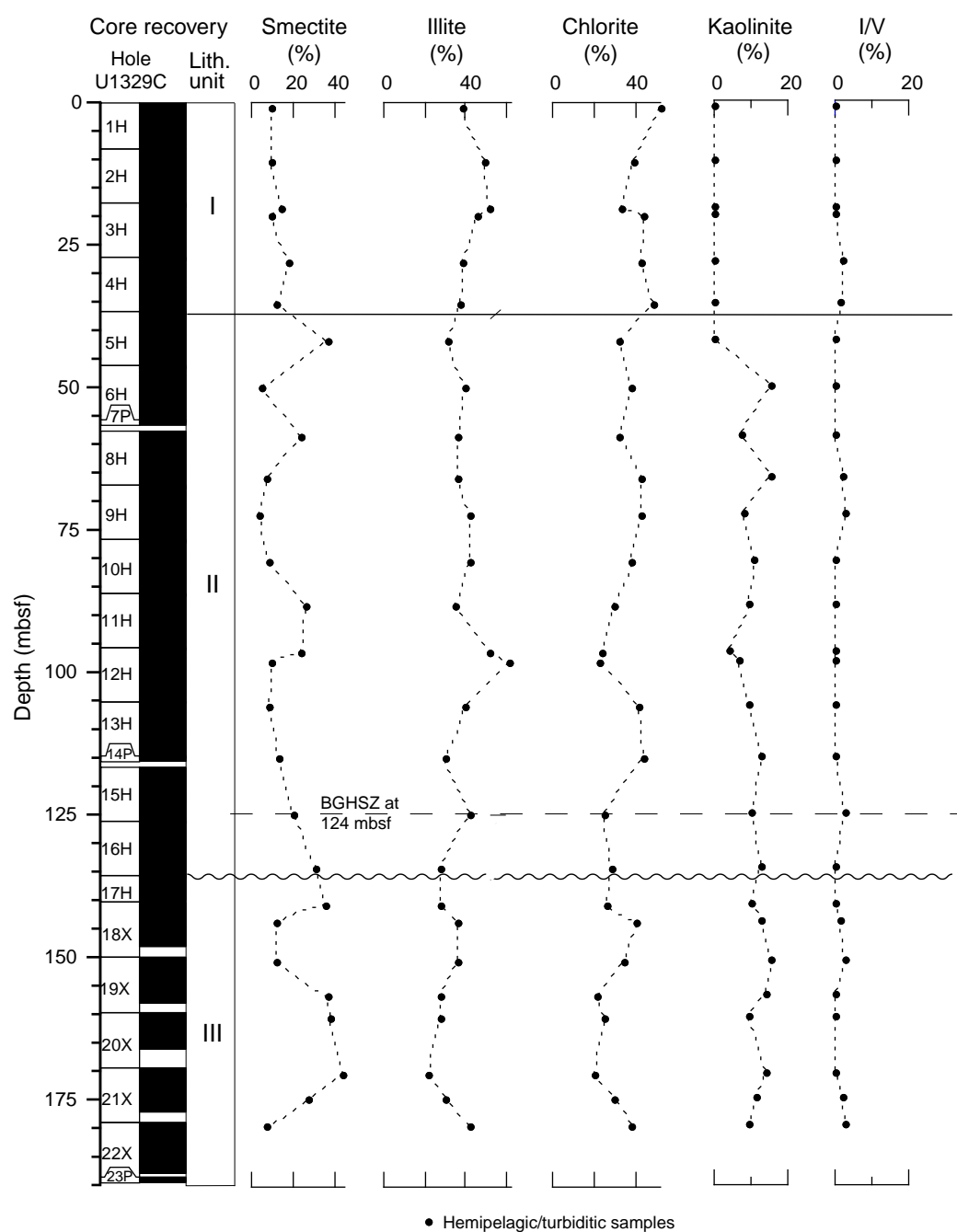


Table T1. X-ray diffractometry mineralogical results of clay fraction (<2 µm). (See table note.) (Continued on next four pages.)

Core, section, interval (cm)	Depth (mbfs)	Lith. unit	X-ray diffraction peak area (total counts)				3.54 Å/3.58 Å	Relative percent (Biscay factors)				Illite/smectite mixed-layer clay				
			Smectite (001)	Illite (001)	Chlorite (002) + Kaolinite (001)	I/V		Smectite	Illite	Chlorite	Kaolinite	I/V	S(001) saddle	S(001) peak	Saddle/Peak	Percent expand
311-U1325B-																
1H-2, 43–45	1.93	IA	145,618	68,651	144,777		2.20	21	39	28	13		4,651	7,751	0.60	66
2H-5, 75–77	16.05	IA	259,790	61,549	206,636	8,981	2.09	28	27	30	14	1	5,659	10,516	0.54	69
4H-1, 75–77	24.75	IB	55,971	123,223	140,234		2.37	7	59	24	10		2,994	4,100	0.73	62
4H-6, 75–77	32.07	IB	90,174	75,099	118,772		2.09	14	48	26	12		3,176	4,817	0.66	65
5H-4, 75–77	38.67	IB	26,435	123,675	116,345		4.98	4	66	26	5		2,557	3,017	0.85	56
6H-3, 75–77	46.75	IB	76,487	58,946	154,994		1.54	12	38	30	20		4,549	6,161	0.74	61
7H-1, 58–60	53.08	II	73,121	56,736	243,164	10,182	2.39	9	28	43	18	1	3,537	5,067	0.70	63
7H-6, 75–77	60.75	II	137,471	62,665	265,222	5,469	2.14	15	27	39	18	1	5,494	8,730	0.63	67
8H-4, 75–77	67.01	II	168,728	96,435	258,315	19,326	2.09	15	35	32	15	2	5,619	8,686	0.65	66
10X-1, 75–77	73.55	II	53,627	163,935	163,436		3.10	5	63	24	8		3,282	4,333	0.76	60
10X-6, 75–77	80.85	II	75,027	75,031	185,627	17,701	3.15	10	39	37	12	2	3,572	5,096	0.70	63
12X-3, 75–77	88.15	II	135,340	81,607	208,182		2.51	15	37	34	13		3,828	6,156	0.62	67
14X-1, 75–77	103.05	III	237,201	105,307	153,204		1.75	25	44	20	12		5,482	10,338	0.53	69
15X-1, 75–77	112.45	III	157,260	90,853	272,221		2.83	15	34	38	13		5,368	9,532	0.56	68
16X-6, 28–30	126.93	III	99,152	64,848	114,464	7,431	1.95	17	44	25	13	1	4,350	5,614	0.77	60
16X-6, 75–77	127.40	III	144,289	113,010	209,551		2.39	14	45	29	12		5,579	8,148	0.68	64
18X-1, 75–77	131.65	III	20,869	44,519	103,725	19,723	2.64	5	42	35	13	5	3,255	3,699	0.88	52
19X-1, 75–77	141.25	III	172,946	63,844	140,501		2.04	24	36	27	13		4,522	7,412	0.61	67
20X-1, 5–7	150.95	III	75,318	72,387	170,879	12,937	2.06	10	40	32	16	2	3,404	4,802	0.71	63
20X-6, 77–79	157.61	III	86,649	76,706	173,265		2.58	12	41	34	13		3,569	5,353	0.67	65
24X-1, 75–77	179.75	III	87,315	97,761	189,630		2.83	10	46	33	12		3,440	4,989	0.69	64
24X-5, 75–77	185.02	III	106,901	73,121	148,334		2.19	15	42	29	13		3,477	5,283	0.66	65
311-U1325C-																
1X-2, 75–77	191.05	III	106,569	106,759	140,831		2.00	13	52	23	12		4,501	5,915	0.76	60
4X-2, 75–77	209.99	IV	60,455	103,162	213,606		2.52	7	46	34	13		3,348	4,392	0.76	60
6X-3, 75–77	221.14	IV	74,045	69,798	235,279	19,858	2.48	9	33	40	16	2	3,512	4,641	0.76	60
6X-4, 75–77	222.26	IV	34,797	72,240	274,089		2.20	4	33	43	20		2,899	3,589	0.81	57
7X-2, 75–77	229.45	IV	96,843	108,868	228,907		2.65	10	44	34	13		3,838	5,218	0.74	61
8X-1, 75–77	237.55	IV	76,429	127,086	189,819		2.98	8	53	29	10		3,492	4,837	0.72	62
8X-6, 75–77	244.05	IV	181,352	129,476	242,878		2.16	15	44	28	13		5,740	8,370	0.69	64
9X-4, 75–77	251.75	IV	64,691	61,926	198,584	22,291	2.26	9	34	38	17	3	3,305	4,174	0.79	58
11X-1, 75–77	257.85	IV	69,961	81,525	233,310	30,489	2.37	8	37	37	16	3	3,688	4,716	0.78	59
11X-2, 75–77	259.35	IV	97,596	104,680	243,781		2.50	10	42	35	14		3,713	5,218	0.71	63
12X-1, 75–77	266.55	IV	72,012	88,193	186,824		2.97	9	44	35	12		3,492	4,495	0.78	59
12X-5, 75–77	272.42	IV	30,027	92,483	137,874		3.96	4	55	33	8		2,649	3,041	0.87	52
15X-1, 75–77	295.45	IV	40,910	69,324	168,694	25,469	4.41	6	41	40	9	4	2,980	3,551	0.84	55
311-U1326C-																
2H-2, 51–53	5.91	I	164,116	86,373	183,646		2.36	19	39	29	12		3,919	6,898	0.57	66
2H-7, 47–49	13.37	I	184,947	96,773	182,747		2.36	20	41	27	12		3,569	7,147	0.50	71
3H-5, 80–82	20.20	I	130,349	83,557	146,273		2.35	17	44	27	12		3,658	5,930	0.62	67
4H-3, 75–77	26.65	II	246,542	46,491	217,004	4,827	1.96	28	21	33	17	1	3,827	9,261	0.41	76
5X-3, 75–77	34.07	II	181,932	75,499	214,827		1.97	20	33	31	16		3,783	7,435	0.51	70
6X-2, 75–77	40.75	II	229,250	52,450	254,623		1.88	24	22	35	19		3,676	8,592	0.43	75
7X-2, 75–77	51.78	II	366,452	55,535	248,878		1.94	34	20	30	16		4,027	12,455	0.32	82
8X-1, 75–77	60.15	II	274,234	48,620	211,380		2.21	31	22	33	15		4,196	10,240	0.41	76
9X-2, 75–77	71.35	II	294,628	67,815	258,571		2.43	27	25	34	14		4,094	10,674	0.38	78
10X-1, 75–77	79.45	II	100,530	95,677	194,758		2.73	12	44	33	12		3,393	5,240	0.65	66

Table T1 (continued). (Continued on next page.)

Core, section, interval (cm)	Depth (mbsf)	Lith. unit	X-ray diffraction peak area (total counts)					3.54 Å/3.58 Å	Relative percent (Biscay factors)					Illite/smectite mixed-layer clay			
			Smectite (001)	Illite (001)	Chlorite (002) + Kaolinite (001)	I/V	Smectite	Illite	Chlorite	Kaolinite	I/V	S(001) saddle	S(001) peak	Saddle/Peak	Percent expand		
311-U1326D-																	
2X-1, 72–74	89.12	II	362,230	36,113	176,236		2.37	42	17	29	12		3,830	12,335	0.31	82	
2X-5, 75–77	95.15	II	181,800	59,203	176,097		2.17	24	31	31	14		4,039	7,310	0.55	68	
3X-3, 75–77	101.85	II	275,328	38,389	208,017		0.88	33	18	23	26		3,997	9,647	0.41	76	
4X-4, 75–77	112.51	II	234,784	55,157	180,762		2.59	29	27	32	12		3,873	9,036	0.43	75	
5X-1, 75–77	118.05	II	123,316	78,569	231,166		2.05	14	35	35	17		3,499	6,054	0.58	67	
5X-6, 75–77	124.35	II	112,230	107,751	258,580		2.41	11	41	34	14		3,499	5,534	0.63	67	
6X-6, 75–77	134.20	II	65,793	91,892	211,449		2.49	8	43	35	14		3,142	4,390	0.72	62	
7X-4, 75–77	140.94	II	41,605	86,350	192,410		2.46	5	45	35	14		2,877	3,644	0.79	58	
8X-3, 75–77	149.51	III	13,466	83,547	155,369	58,382	3.55	2	47	34	10	8	2,507	2,746	0.91	49	
9X-1, 75–77	156.65	III	89,771	35,631	120,886		2.27	19	30	35	16		3,589	5,513	0.65	66	
10X-1, 75–77	166.35	III	92,678	58,173	168,618		2.37	14	35	36	15		3,629	5,378	0.67	65	
10X-4, 75–77	170.77	III	75,167	48,856	124,775		2.59	14	38	35	13		3,092	4,364	0.71	63	
11X-4, 75–77	179.44	III	19,508	44,792	253,182	7,808	2.24	3	25	49	22	1	2,405	2,820	0.85	56	
12X-2, 75–77	186.80	III	48,686	98,675	169,288		2.69	6	50	32	12		3,106	4,032	0.77	60	
13X-1, 75–77	195.15	III	14,861	53,520	233,263	6,955	2.49	2	30	47	19	1	2,575	2,887	0.89	51	
14X-1, 75–77	204.75	III	39,956	94,068	202,596	22,906	3.01	5	45	36	12	3	3,162	3,991	0.79	58	
15X-1, 73–75	214.33	III	41,741	109,397	202,723		3.12	5	49	35	11		2,933	3,863	0.76	60	
16X-1, 75–77	224.05	III	71,390	109,103	218,355		2.64	8	46	34	13		3,423	4,619	0.74	61	
17X-1, 75–77	233.65	III	25,527	90,374	154,120		2.38	4	52	31	13		2,981	3,449	0.86	54	
17X-3, 0–100	235.90	III	58,815	53,093	170,389	23,825	2.65	9	33	39	15	4	3,618	4,664	0.78	59	
17X-5, 75–77	239.65	III	25,490	58,856	244,420	10,365	3.02	3	31	48	16	1	3,133	3,599	0.87	52	
20X-3, 75–77	264.50	III	105,108	101,827	192,621		2.57	12	45	31	12		3,974	5,592	0.71	63	
20X-7, 74–76	269.78	III	39,121	80,237	154,762		2.52	6	48	33	13		3,011	3,596	0.84	55	
311-U1327C-																	
1H-2, 75–77	2.25	I	256,280	76,041	219,424	10,687	2.40	25	30	31	13	1	5,375	10,310	0.52	69	
2H-2, 75–77	8.35	I	150,519	73,697	182,232	8,003	2.60	18	36	32	12	1	7,392	8,892	0.83	56	
3H-1, 75–77	16.35	I	102,230	72,625	144,826	7,418	2.10	15	42	28	14	1	7,114	7,714	0.92	49	
3H-5, 75–77	22.35	I	40,443	91,460	169,793	27,361	2.36	5	47	31	13	4	5,861	6,012	0.97	46	
4H-3, 75–77	28.85	I	125,152	56,550	156,475	4,702	1.95	19	34	31	16	1	6,580	8,143	0.81	57	
5H-3, 75–77	38.35	I	101,917	70,061	234,295	17,652	3.20	12	32	41	13	2	7,061	7,818	0.90	50	
7H-2, 75–77	48.35	I	170,263	70,703	187,573		2.07	21	34	31	15		7,747	10,047	0.77	60	
8H-1, 75–77	56.35	I	268,308	63,666	226,219		2.07	28	26	31	15		7,810	12,496	0.63	66	
9H-1, 75–77	65.85	I	97,992	94,034	202,779	21,951	2.55	11	42	32	13	2	7,470	7,980	0.94	47	
9H-6, 75–77	73.35	I	46,766	49,138	119,787	18,302	2.60	9	39	35	13	4	6,667	6,979	0.96	45	
10H-1, 96–98	75.56	I	157,834	68,649	193,434		1.94	19	34	31	16		4,085	6,668	0.61	67	
10H-6, 75–77	81.50	I	135,678	80,194	233,227	18,679	2.35	14	34	35	15	2	7,787	9,011	0.86	52	
11H-4, 75–77	89.35	I	53,315	72,592	172,086	20,533	2.22	8	41	34	15	3	6,421	6,686	0.96	45	
12X-6, 75–77	99.87	II	238,076	95,343	171,022		1.90	25	40	23	12		5,285	9,599	0.55	69	
13X-4, 75–77	107.75	II	62,793	68,972	156,312	16,894	2.66	9	41	34	13	3	6,584	7,043	0.93	48	
14X-3, 75–77	115.85	II	71,740	109,004	215,572		2.55	8	46	33	13		6,371	7,037	0.91	49	
16X-1, 75–77	124.55	II	56,280	58,947	144,569	10,518	2.29	10	40	34	15	2	7,043	7,433	0.95	46	
16X-3, 75–77	127.45	II	109,329	69,252	217,386	10,097	2.36	13	33	37	16	1	6,125	7,714	0.79	58	
18X-1, 72–74	142.22	II	144,492	40,693	84,663	2,764	2.64	30	34	26	10	1	7,493	8,829	0.85	56	
18X-2, 0–5	142.35	II	118,421	33,198	75,488		2.44	29	33	27	11		4,166	5,711	0.73	62	
18X-2, 130–150	143.65	II	101,190	40,889	101,571		2.01	22	35	29	14		3,940	5,326	0.74	61	
19X-1, 75–77	151.85	II	98,030	39,034	105,135		2.11	21	34	31	15		6,673	7,573	0.88	52	
19X-6, 75–77	158.35	II	118,905	51,388	104,528		2.21	22	39	27	12		7,442	8,275	0.90	50	
20X-3, 75–77	163.83	II	167,713	70,924	178,998		1.79	21	35	28	16		4,577	7,278	0.63	66	

Table T1 (continued). (Continued on next page.)

Core, section, interval (cm)	Depth (mbsf)	Lith. unit	X-ray diffraction peak area (total counts)					3.54 Å/3.58 Å	Relative percent (Biscay factors)					Illite/smectite mixed-layer clay			
			Smectite (001)	Illite (001)	Chlorite (002) + Kaolinite (001)		I/V		Smectite	Illite	Chlorite	Kaolinite	I/V	S(001) saddle	S(001) peak	Saddle/Peak	Percent expand
21X-1, 75–77	171.15	III	97,114	89,810	189,757			2.42	12	43	32	13		3,555	5,298	0.67	65
21X-6, 75–77	178.17	III	62,099	55,319	103,942			2.61	13	45	31	12		6,666	7,178	0.93	48
21X-7, 0–1	178.43	III	83,827	78,057	107,581			2.62	14	51	25	10		4,181	5,244	0.80	58
22X-5, 75–77	186.00	III	44,466	68,416	185,137	15,499		2.73	6	39	39	14	2	2,998	3,788	0.79	58
25X-2, 77–79	200.88	III	43,317	84,157	151,989			2.50	6	49	32	13		2,883	3,335	0.86	53
26X-1, 75–77	209.65	III	59,274	161,121	225,754			4.02	5	56	31	8		3,522	4,442	0.79	58
27X-1, 75–77	219.25	III	67,246	90,811	161,406			3.20	9	48	33	10		6,642	7,314	0.91	49
27X-5, 75–77	224.88	III	298,684	76,204	167,537			2.12	32	32	24	11		4,798	10,453	0.46	73
28X-2, 74–76	230.34	III	97,648	87,679	205,050			2.31	11	41	33	14		3,463	4,988	0.69	64
29X-1, 75–77	238.45	III	46,829	92,360	106,892			3.11	7	59	26	8		2,643	3,435	0.77	60
29X-5, 75–77	244.30	III	55,605	73,855	139,283	21,377		2.94	9	45	32	11	3	3,461	4,258	0.81	57
30X-5, 70–72	253.31	III	109,979	144,143	282,440			3.10	9	46	34	11		4,157	6,008	0.69	64
31X-5, 75–77	263.81	III	109,335	24,891	60,971			2.11	33	30	25	12		6,776	7,318	0.93	48
32X-2, 75–77	268.95	III	69,442	140,233	177,811			3.11	7	57	27	9		3,094	4,213	0.73	62
33X-2, 75–77	278.55	III	53,202	109,003	95,289			2.62	8	64	20	8		3,192	3,867	0.83	56
34X-2, 77–79	288.17	III	92,256	125,531	137,241			3.47	11	58	25	7		3,715	5,365	0.69	64
35X-1, 75–77	296.25	III	107,844	45,510	95,624			3.20	22	38	30	9		3,659	5,380	0.68	64
311-U1327D-																	
5X-1, 65–75	126.95	II	45,362	93,425	128,511			2.38	7	55	27	11		2,893	3,620	0.80	58
11X-1, 0–8	157.10	II	20,965	54,134	50,421			2.69	6	64	22	8		2,312	2,709	0.85	56
311-U1328B-																	
1H-1, 71–73	0.71	I	23,999	23,958	34,872			2.23	13	51	25	11		963	1,394	0.69	64
1H-3, 60–62	3.60	I	38,356	36,976	34,052			2.07	15	58	18	9		1,084	1,768	0.61	67
4P-1, 0–11	14.50	I	88,812	29,316	44,333			1.54	30	40	18	12		1,751	3,303	0.53	69
5H-1, 68–70	17.18	I	15,671	30,550	52,685			2.37	6	50	30	13		965	1,228	0.79	58
6X-1, 0–20	18.40	I	74,851	22,912	50,147			1.59	28	34	23	15		1,545	2,920	0.53	69
6X-1, 36–38	18.76	I	29,223	20,304	51,742			2.42	14	38	34	14		1,093	1,611	0.68	64
8H-1, 75–77	28.75	I	21,903	44,514	60,169			2.44	7	56	27	11		1,159	1,594	0.73	62
9H-1, 75–77	38.25	I	26,444	27,352	41,728			1.93	12	50	25	13		1,021	1,519	0.67	65
9H-6, 75–77	45.56	I	26,421	18,444	44,493			2.09	14	39	32	15		1,022	1,556	0.66	65
10H-5, 75–77	53.75	I	28,584	20,727	55,875			2.71	13	37	37	13		1,053	1,580	0.67	65
311-U1328C-																	
1H-4, 75–77	61.68	I	21,064	13,535	45,013	3,247		2.47	13	32	38	15	2	1,010	1,442	0.70	63
2H-5, 75–77	72.75	I	13,002	13,258	26,838	2,573		2.58	11	43	32	12	2	927	1,114	0.83	56
3H-6, 76–78	83.76	I	32,634	22,948	54,651			2.23	14	39	32	14		1,153	1,701	0.68	64
6H-1, 75–77	94.75	I	15,956	23,826	55,491	3,194		2.23	7	42	34	15	1	984	1,293	0.76	60
6H-6, 75–77	99.75	I	61,107	15,442	33,451			2.22	32	33	24	11		1,219	2,320	0.53	69
6H-8, 75–77	102.14	I	60,680	23,373	39,939			1.69	26	40	21	13		1,139	2,370	0.48	72
7X-1, 73–75	104.23	I	34,786	18,855	23,735			2.02	22	48	20	10		1,055	1,674	0.63	67
7X-4, 75–77	108.65	I	59,885	7,647	46,093			2.91	33	17	38	13		1,120	2,538	0.44	74
8X-2, 74–76	112.54	I	50,878	14,529	52,789	1,012		3.56	24	27	38	11	1	1,156	2,211	0.52	69
9X-1, 78–80	120.68	I	48,701	8,043	37,589	1,504		1.89	31	20	31	16	1	1,077	2,114	0.51	70
9X-4, 72–74	124.62	I	71,345	14,832	49,130			2.56	31	26	31	12		1,071	2,482	0.43	75
9X-5, 78–80	126.18	I	94,370	13,061	52,412			3.42	38	21	32	9		1,271	3,404	0.37	79
10X-1, 75–77	130.35	I	49,817	16,905	40,313			2.17	25	34	28	13		1,158	2,087	0.55	71
10X-3, 75–77	133.35	II	11,847	33,677	24,573			3.59	6	69	20	5		845	1,041	0.81	57
11X-1, 75–77	140.05	II	32,020	21,293	27,659			2.42	19	49	23	9		1,131	1,659	0.68	64
11X-2, 75–77	141.55	II	25,981	14,257	23,009			2.93	20	44	27	9		1,051	1,452	0.72	62

Table T1 (continued). (Continued on next page.)

Core, section, interval (cm)	Depth (mbsf)	Lith. unit	X-ray diffraction peak area (total counts)					3.54 Å/3.58 Å	Relative percent (Biscay factors)					Illite/smectite mixed-layer clay			
			Smectite (001)	Illite (001)	Chlorite (002) + Kaolinite (001)	I/V	Smectite	Illite	Chlorite	Kaolinite	I/V	S(001) saddle	S(001) peak	Saddle/Peak	Percent expand		
12X-1, 75–77	149.65	II	15,223	18,756	36,735	2,662	2.89	9	45	33	11	2	951	1,223	0.78	59	
13X-1, 75–77	159.35	II	15,500	23,961	50,446		2.49	7	45	34	14		937	1,164	0.80	58	
13X-2, 75–77	160.82	II	18,391	16,388	38,601	5,066	2.26	11	39	32	14	3	962	1,268	0.76	60	
14X-2, 75–77	170.28	II	4,962	17,628	38,189	8,482	2.46	3	44	34	14	5	845	963	0.88	52	
15X-2, 75–77	180.15	II	7,260	16,440	39,341	3,809	2.76	5	42	37	13	2	833	989	0.84	55	
15X-5, 75–77	184.62	II	8,414	28,811	41,299		2.79	4	56	29	11		864	995	0.87	52	
16X-5, 75–77	194.25	II	13,527	29,640	40,495		2.98	6	56	28	10		970	1,225	0.79	58	
17X-4, 75–77	202.35	III	15,743	22,033	41,130	4,059	2.62	8	46	31	12	2	1,001	1,524	0.66	65	
19X-2, 75–77	217.78	III	28,705	20,793	48,814	5,452	2.74	13	39	33	12	3	1,230	1,746	0.70	63	
19X-4, 24–26	220.27	III	34,560	16,052	45,978	1,532	2.54	18	33	34	13	1	1,379	1,938	0.71	63	
19X-4, 32–36	220.35	III	48,771	19,476	47,399		2.50	22	35	31	12		1,480	2,183	0.68	64	
19X-4, 77–79	220.80	III	20,084	30,026	39,573		2.42	9	55	26	11		1,037	1,439	0.72	62	
20X-3, 75–77	229.10	III	6,400	8,899	26,289	4,997	4.01	6	36	42	11	5	766	850	0.90	50	
20X-5, 75–77	231.82	III	12,636	34,695	42,217		2.51	5	59	26	10		944	1,667	0.57	67	
22X-5, 75–77	251.06	III	9,815	11,507	30,915	1,379	2.91	8	39	39	13	1	870	1,037	0.84	55	
22X-6, 75–77	252.56	III	35,738	38,584	57,542		3.20	12	51	29	9		1,313	1,966	0.67	65	
22X-CC, 12–14	253.70	III	16,131	5,888	27,746		3.70	17	25	46	12		1,025	1,191	0.86	54	
25X-1, 78–80	274.88	III	47,449	16,345	11,613		2.27	35	48	12	5		1,205	1,994	0.60	66	
25X-2, 77–79	276.37	III	25,658	13,277	43,862		2.04	15	32	35	17		1,107	1,454	0.76	60	
26X-2, 73–75	285.93	III	17,508	22,794	42,050		2.30	9	47	30	13		921	1,245	0.74	61	
26X-4, 71–73	288.91	III	30,005	9,723	25,391		2.65	25	32	31	12		1,124	1,592	0.71	63	
27X-5, 75–77	299.86	III	8,180	9,410	21,533	1,923	2.87	9	41	35	12	2	770	904	0.85	56	
311-U1329B-1H-1, 74–76	0.74	I	64,624	69,838	186,089			9	39	52			3,134	4,364	0.72	62	
311-U1329C-2H-2, 75–77	10.35	I	57,732	81,182	122,863			9	52	39			2,731	3,724	0.73	62	
3H-1, 77–79	18.37	I	116,637	104,382	135,706			14	52	34			3,629	5,669	0.64	66	
3H-2, 75–77	19.85	I	76,719	97,657	178,766			9	47	43			3,373	4,977	0.68	64	
4H-1, 75–77	27.85	I	131,347	70,991	157,480	17,344		18	38	42		2	4,907	6,954	0.71	63	
4H-6, 75–77	35.35	I	85,700	67,819	169,943	8,816		12	38	48		1	4,114	5,653	0.73	62	
5H-4, 74–76	41.84	II	222,962	46,764	98,343			37	31	32			5,786	9,231	0.63	67	
6H-3, 75–77	49.85	II	37,733	77,041	199,485			2.47	5	41	38	15		2,629	3,251	0.81	57
8H-1, 75–77	58.35	II	110,566	42,405	91,575			4.20	24	37	32	8		3,385	5,245	0.65	66
8H-6, 75–77	65.85	II	46,182	49,413	177,854	13,950		2.85	8	32	43	15	2	2,835	3,757	0.75	61
9H-4, 75–77	72.35	II	22,468	67,301	157,344	18,966		5.08	4	43	42	8	3	2,409	2,810	0.86	54
10H-3, 75–77	80.35	II	62,402	85,987	195,504			3.65	8	43	38	11		3,066	4,153	0.74	61
11H-2, 75–77	88.35	II	126,721	43,240	94,754			3.03	26	35	29	10		3,501	5,748	0.61	67
12H-1, 75–77	96.35	II	89,971	47,571	52,866			5.65	23	49	23	4		2,754	4,428	0.62	67
12H-2, 75–77	97.83	II	87,409	143,721	134,903			3.15	9	62	22	7		3,151	4,873	0.65	66
13H-1, 75–77	105.85	II	61,366	77,707	190,995			4.34	8	41	41	9		3,073	4,207	0.73	62
13H-7, 72–74	114.82	II	99,066	61,797	222,271			3.45	13	31	44	13		3,372	5,549	0.61	67
15H-6, 75–77	124.85	II	117,222	59,916	98,035	14,708		2.54	21	42	25	10	3	4,027	5,606	0.72	62
16H-6, 75–77	134.35	II	127,120	29,156	83,225			2.27	31	28	28	12		3,641	5,783	0.63	67
18X-1, 57–59	140.77	III	134,316	26,306	69,069			2.65	36	28	27	10		3,442	5,467	0.63	67
18X-3, 57–59	143.77	III	71,262	51,703	164,080	8,654		3.22	12	34	41	13	1	3,312	4,728	0.70	63
19X-1, 75–77	150.65	III	66,437	48,373	133,423	14,346		2.26	12	36	34	15	3	3,358	4,255	0.79	58
19X-5, 75–77	156.65	III	173,344	33,014	84,684			1.52	37	28	22	14		4,191	6,766	0.62	67
20X-1, 75–77	160.35	III	230,447	42,628	103,176			2.56	38	28	24	10		4,516	8,444	0.53	69
21X-1, 75–77	170.05	III	341,626	40,409	132,606			1.40	44	21	20	14		4,765	10,596	0.45	73

Table T1 (continued).

Core, section, interval (cm)	Depth (mbsf)	Lith. unit	X-ray diffraction peak area (total counts)				3.54 Å/ 3.58 Å	Relative percent (Biscay factors)					Illite/smectite mixed-layer clay			
			Smectite (001)	Illite (001)	Chlorite (002) + Kaolinite (001)	I/V		Smectite	Illite	Chlorite	Kaolinite	I/V	S(001) saddle	S(001) peak	Saddle/ Peak	Percent expand
21X-4, 75–77	174.55	III	173,603	46,488	129,327	13,857	2.59	27	29	30	11	2	4,322	7,318	0.59	67
22X-1, 55–57	179.45	III	49,875	72,519	159,794	20,036	3.84	7	43	37	10	3	3,248	4,015	0.81	57

Note: I/V = illite/vermiculite mixed layers.

